

Article

Geological Significance of Neoproterozoic Intrusive Rocks in the South Section of the Ailaoshan Orogenic Belt, SW China: Insights from Petrology, Geochemistry, and Geochronology

Yaoyao Zhang ^{1,2} , Da Zhang ^{2,*}, Kai Liu ^{1,*}, Xuanxue Mo ², Shuxun Wang ^{1,2}, Zenan Zhao ³, Xiaolong He ⁴  and Tingxi Yu ^{1,2} 

¹ Chinese Academy of Geological Sciences, China Geological Survey, Ministry of Natural Resources, Beijing 100037, China

² School of Earth Sciences and Resources, China University of Geosciences (Beijing), Beijing 100083, China

³ Hebei Regional Geological Survey Institute, Langfang 065000, China

⁴ School of Environment and Resources, Xiangtan University, Xiangtan 411105, China

* Correspondence: zhangda@cugb.edu.cn (D.Z.); acancer@163.com (K.L.)

Abstract: The Ailaoshan orogenic belt is one of the most significant orogenic belts in the southeastern margin of the Qinghai–Tibet Plateau. The widely developed magmatic rocks in this belt preserve the multi-stage tectonic evolution records of the South China Plate. As an important response to the Rodinia breakup tectonic event, the study of Neoproterozoic magmatic rocks in the area is of great significance for reconstructing the Neoproterozoic tectonic process of the Ailaoshan orogenic belt and the tectonic evolution of the South China Plate. Petrology, geochemistry, zircon U–Pb, and Lu–Hf isotopes of the Daping pluton in the Ailaoshan orogenic belt are studied in this paper. The Daping pluton is mainly divided into gabbros and granites. Gabbros and granites belong to the sub-alkaline series, which are relatively enriched in large ion lithophilic elements and depleted in high-field strength elements. The Σ REE contents of the gabbro are low with enrichment in LREEs and depletion in HREEs, and the degree of differentiation of light and heavy rare earth is low, with positive δ Eu and weak negative δ Ce anomalies. The Σ REE contents of the granite are low with enrichment in LREEs and depletion in HREEs, and the degree of light and heavy rare earth differentiation is high, with medium–weak negative δ Eu and weak positive δ Ce anomalies, suggesting an A₂-type granite with A₁–A₂ transition characteristics. The weighted average age of the gabbro is 816.1 ± 4.1 Ma (MSWD = 0.11), with zircon $\varepsilon_{\text{Hf}}(t)$ values of -7.5 – -5.5 . The magma source is a mixture of an ancient crust source and a new mantle source; the weighted average age of the syenogranite is 783.7 ± 8.1 Ma (MSWD = 1.4), with zircon $\varepsilon_{\text{Hf}}(t)$ values of -4.3 – -0.4 . The magma source is mainly ancient crustal material (Ailaoshan Group), mixed with a small amount of mantle-derived material; the weighted average age of the monzogranite is 754.8 ± 6.1 Ma (MSWD = 3.0), with positive zircon $\varepsilon_{\text{Hf}}(t)$ values of 1.65 – 10.36 . The magma source is a mixture of a large number of mantle-derived materials and a small number of crust-derived materials (Ailaoshan Group). The Daping pluton was formed in the transitional tectonic environment from post-collision to intraplate continental margin rift, corresponding to the Rodinia breakup process in the western margin of the South China Plate.

Keywords: Ailaoshan orogenic belt; intrusive rocks; A-type granite; geochronology; Neoproterozoic



Citation: Zhang, Y.; Zhang, D.; Liu, K.; Mo, X.; Wang, S.; Zhao, Z.; He, X.; Yu, T. Geological Significance of Neoproterozoic Intrusive Rocks in the South Section of the Ailaoshan Orogenic Belt, SW China: Insights from Petrology, Geochemistry, and Geochronology. *Minerals* **2023**, *13*, 349. <https://doi.org/10.3390/min13030349>

Academic Editor: Stefano Salvi

Received: 8 February 2023

Revised: 27 February 2023

Accepted: 28 February 2023

Published: 1 March 2023



Copyright: © 2023 by the authors. Licensee MDPI, Basel, Switzerland. This article is an open access article distributed under the terms and conditions of the Creative Commons Attribution (CC BY) license (<https://creativecommons.org/licenses/by/4.0/>).

1. Introduction

The Rodinia is a supercontinent that existed on the earth in the early Neoproterozoic era, and the breakup of Rodinia is one of the hot topics in global tectonic and Precambrian geological research. The concept of Neoproterozoic ‘Rodinia’, proposed by McMenamin and McMenamin [1], was a global supercontinent formed by continental collision before 1.00 Ga. Previously, researchers have achieved great achievements in paleomagnetism, magmatic rocks, isotope chronology, stratigraphy, and so on. Hoffman [2] established

a supercontinent reconstruction map based on paleomagnetic data. Paleomagnetic data indicated that Rodinia was formed in the late Mesoproterozoic era, during the formation of the global Greenwell orogenic belt at 1.10 Ga, through the mutual collage of ancient cratons [3,4]. Isotopic chronological data indicated that the collision among the East Antarctic Craton, other Australian cratons, and the Gawler Craton occurred at 1.50–1.55 Ga and Australia entered the initial collage period [5–7]. Li et al. [3,4] proposed that the South China Plate (Yangtze and Cathaysian) was located between the Australia and Lauren continents based on the geochronological and stratigraphic data of the orogenic belt, which is the bridge connecting North America and the Australia–Antarctic continent and the core of Rodinia.

The South China Plate has a large space–time span and records a relatively complete tectonic evolution history since the Proterozoic era. It is one of the key areas for the study of the reconstruction of the Rodinia. Some researchers believed that significant rifting occurred after about 820 Ma in the South China Plate and formed the Neoproterozoic–Paleozoic South China rift system [8,9]. The center of the South China rift was roughly located at the current northern Guangxi–central (southern) Hunan–northern Jiangxi–northeastern Zhejiang and Kangdian area, and the starting time of the rift was nearly 820–800 Ma [10]. Widespread basaltic rocks around the Yangtze Block [11–14] indicated that the Cathaysia Block began to break up at the Neoproterozoic era (830–800 Ma). Other geological and geochronological research shows that the ancient Cathaysia Block was in a continental margin rift environment during 808–690 Ma (Figure 1; [15–21]).

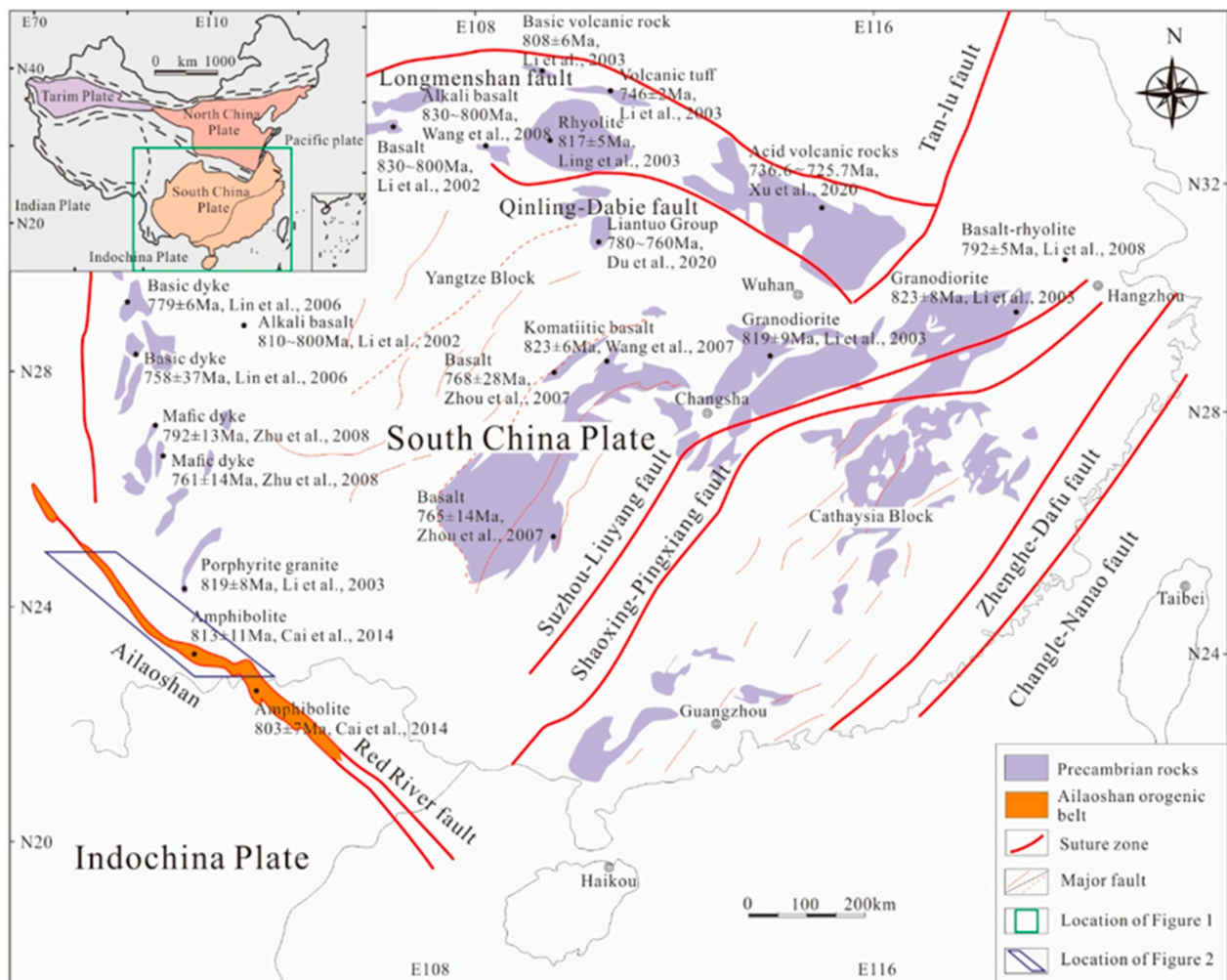


Figure 1. Simplified geotectonic map showing the location of the Ailaoshan orogenic belt (modified after [8,12,13,15,18–22]).

Previous studies established an important basis for the breakup of Rodinia. However, there are relatively few studies on the breakup of Rodinia in the Ailaoshan area at the southwestern margin of the South China Plate. Cai et al. [22] proposed that the subduction in this area occurred in the Neoproterozoic era. At the same time, there is great controversy about the formation age of the Daping pluton which mainly involves the Ordovician [23,24] and the Neoproterozoic periods [25–27]. This study suggests that, except for the Daping gabbro, the newly discovered syenogranite and monzogranite are also the products of the Neoproterozoic magmatic activity. Based on the study of petrology, geochemistry, zircon U-Pb isotope, and Lu-Hf isotope, this paper is aimed to determine the formation ages of the two intrusive rocks of Daping gabbro and granite and identify the magma source and discuss its tectonic significance.

2. Regional Geological Setting

The Ailaoshan orogenic belt is located in the southeastern part of the Sanjiang area in southwest China and on the west side of the South China Plate [28–33]. The Indian and Eurasian Plates had experienced multiple openings and closings, expansions, mergings, and extrusions, which led to the formation of the Ailaoshan orogenic belt. Due to long-term tectonic evolution, the orogenic belt is broom-shaped and located between the Yangtze block and the Indochina block [34,35]. The Ailaoshan orogenic belt starts from Midu in the northwest and extends abroad through the Jinping area in the southeast. The area is located in the tectonic–magma–metamorphic zone between three fault zones, narrow in the northwest and wide in the southeast (Figure 2a).

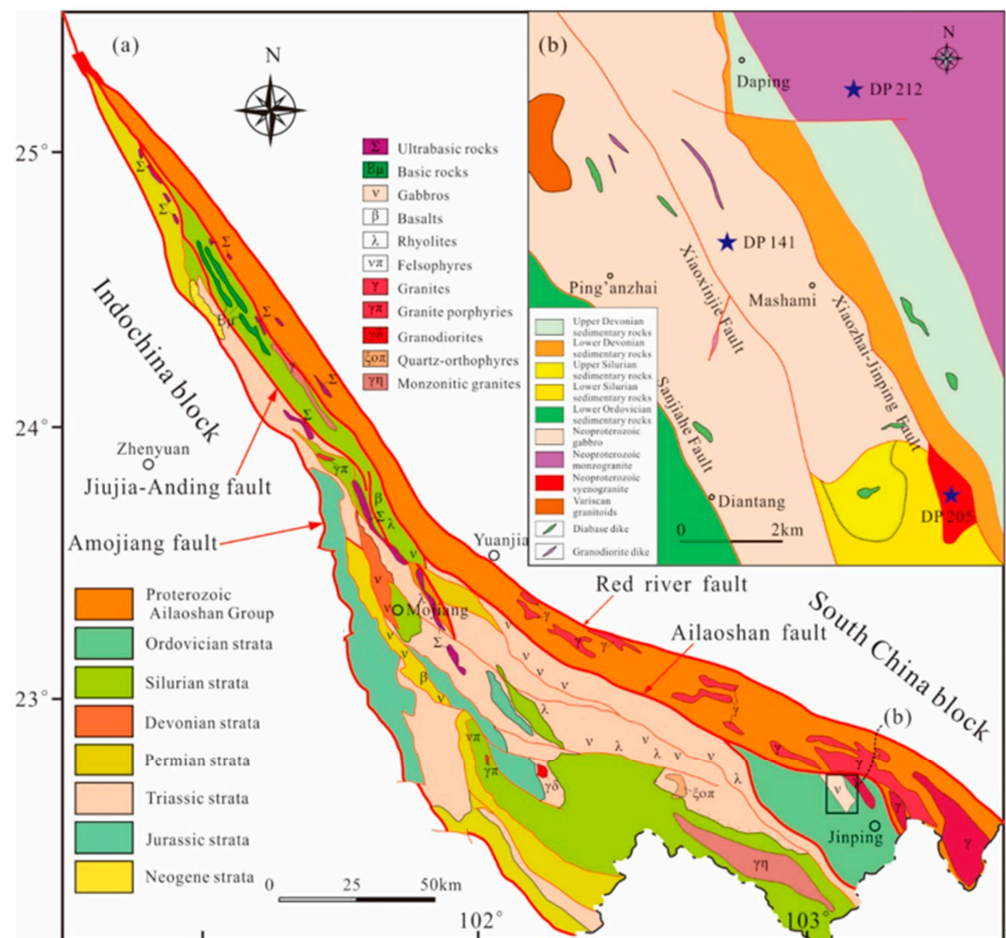


Figure 2. (a) Schematic geological map of the Ailaoshan orogenic belt showing (b) the distribution of the Daping pluton.

The exposed stratum is bounded by the Ailaoshan fault, and the NE stratum is the lower Proterozoic deep metamorphic belt–Ailaoshan group; the SW stratum is the Paleozoic shallow metamorphic belt, and the Mesozoic and Cenozoic strata are above it [36]. The Ailaoshan rock group includes the Xiaoyangjie Formation (Pt_{1x}), A'long Formation (Pt_{1a}), Fenggang Formation (Pt_{1f}), and Wudukeng Formation (Pt_{1w}). The lithology of the lower part of the Xiaoyangjie Formation is mainly two-mica schist and biotite granulite, and the upper part is mainly biotite plagioclase gneiss and biotite amphibolite. The lower part of the A'long Formation is mainly hornblende plagioclase gneiss and hornblende granulite, and the upper part are mainly marble and biotite hornblende granulite. The lithology of the lower part of the Fenggang Formation is mainly sillimanite–biotite monzonitic gneiss and garnet–biotite amphibolite, and the lithology of the middle–upper part is mainly plagioclase amphibolite and garnet plagioclase amphibolite. The lower part of the Wudukeng Formation is mainly migmatized biotite plagioclase gneiss and biotite amphibole plagioclase gneiss, and the upper part is mainly quartz schist and marble.

The magmatic activity in this area has the characteristics of multi-period and long-term, from Neoproterozoic to Himalayan. From ultrabasic rocks to alkaline rocks, rocks have characteristics of multiple types. The output form, scale, and distribution of rocks are restricted and controlled by three deep faults (Red River fault, Ailaoshan fault, and Amojiang fault). The acid rocks are widely developed, mainly exposed on the northeast and southwest sides of the Ailaoshan fault, and secondly distribute along the Jiujiia–Anding fault.

3. Samples and Methods

3.1. Sample Collection and Features

Gabbro and granites are distributed in the Daping area with a large exposed range. Granites include syenogranite and monzogranite. The gabbro pluton is strongly reformed by multiple tectonic processes. The granite pluton is subjected to late metamorphism–deformation, and the rock has mylonitization characteristics (Figure 2b).

The gabbro is light gray, fine–medium granular, and semi-automorphic granular texture, mainly composed of plagioclase and hornblende (Figure 3a). The plagioclase is mainly a self-shaped plate with a content of 50–55%. Only a few hornblendes are semi-automorphic short columnar, and most of them are filled between plagioclase, with a content of 30–35% (Figure 3b). Hornblende has strong polychromism and absorbency. Apatite and zircon inclusions are common in fissures. The secondary minerals are biotite and quartz. The biotite is derived from amphibole with a content of about 4%. Quartz generally has wavy extinction, with a content of <5%.

The syenogranite is light gray, with a granite texture and massive structure (Figure 3c). The rock consists of potassium feldspar, quartz, plagioclase, and biotite (Figure 3d). Potassium feldspar is often yellowish-white, and the crystals are short columnar, which have a content of 45–50%. Quartz is anhedral granular, colorless, and transparent, with weak wavy extinction, and the content is about 20–30%. The columnar plagioclase develops a polysynthetic twin, with a content of 10–15%. Biotite is iron-rich dark brown, with typical biotite absorption, and the content is 12–15%. The accessory minerals are magnetite, apatite, ilmenite, zircon, and monazite.

The monzogranite is light-gray or gray-white, with a granite texture and massive structure (Figure 3e). The rock is composed of potassium feldspar, plagioclase, quartz, biotite, and muscovite (Figure 3f). Potassium feldspar is mainly in the form of a nearly subhedral plate, with a small number of anhedral particles, partly kaolinization. Its particle size is mostly 2–5 mm, and the content is 35–40%. The plagioclase is in the form of a subhedral plate that is anhedral granular; its grain size generally varies from 0.4 to 3.0 mm, with sericitization and epidotization, which has a content of 25–30%. The biotite and muscovite are in scaly-leaf shape, and the diameter is generally less than 1.0 mm. Biotite has chloritization, with a biotite content of 4% and muscovite content of about 2%.

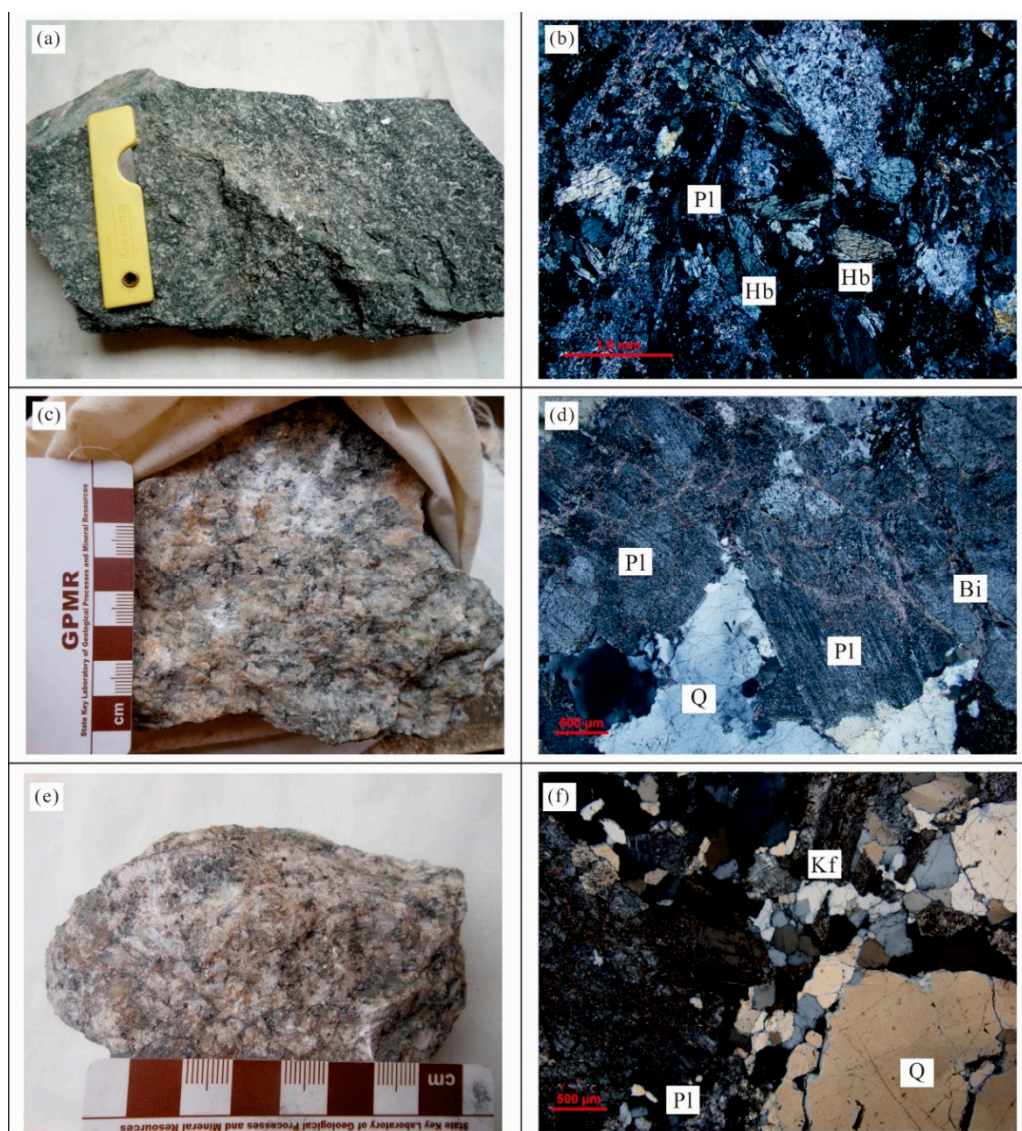


Figure 3. Hand specimen, and micrograph of magmatic rocks. (a)—Photograph of hand specimen of gabbro (DP-141) used for zircon U-Pb dating; (b)—Orthogonal polarizing photo of gabbro (DP-141); (c)—Photograph of hand specimen of syenogranite (DP-205) used for zircon U-Pb dating; (d)—Orthogonal polarizing photo of syenogranite (DP-205); (e)—Photograph of hand specimen of monzogranite (DP-212) used for zircon U-Pb dating; (f)—Orthogonal polarizing photo of monzogranite (DP-212). Pl—plagioclase; Hb—hornblende; Q—quartz; Bi—biotite; Kf—K-feldspar.

3.2. Experimental Methods

Based on a detailed field geological survey, fresh weakly altered samples were taken for petrology, geochemistry, isotope chronology, Hf isotope, and other research. The sampling locations are shown in Figure 2b.

The geochemical analysis of the rock samples was performed in the laboratory of the Institute of Geophysical and Geochemical Exploration, Chinese Academy of Geological Sciences. The analysis method of major elements was XRF, and the implementation standard was GB/B14506.28~1993. The analysis of H_2O^+ accorded to GB/T14506.2~1993, and the loss on ignition standard was LY/T1253-1999; the rare earth element analysis method was ICP-MS, with the standard of DZ/T0223-2001. The trace elements were tested by X-ray fluorescence spectrometer 2100, according to standard JY/T016-1996, and the test accuracy met the requirements.

Zircons were sorted and targeted at Hebei District Survey Institute. The analysis of transmission, reflection, and cathodoluminescence (CL) was completed in Beijing Zirconia Pilot Technology Co., Ltd., China. Zircon dating analyses were completed in the laboratory of Tianjin Geological Survey Center, China Geological Survey. The laser ablation multi-receiver inductively coupled plasma mass spectrometer (LA-ICP-MS) was used as the analytical instrument. The laser wavelength was 193 nm, the laser energy density was 13–14 J·cm⁻², and the frequency of 8–10 Hz. The laser ablation spot diameter was 35 µm and the laser ablation material entered Neptune with helium as the carrier gas. Plesovice (age of 337 ± 0.37 Ma) [37] was used as the external standard for correction. Common lead calibration used the ComPbCorr#3.17 calibration procedure [38]. The data processing was carried out by the ICP-MS DataCal program and the Isoplot program. The weighted average age of zircon was calculated and the Concordia plot was drawn. Detailed instrument operating conditions and data processing methods are shown in Liu et al. [39].

Zircon Hf isotope analysis was also performed on the LA-ICP-MS at the isotope laboratory of Tianjin Geological Survey Center, China Geological Survey. The laser ablation system is the UP193FX193nm ArF excimer system, which is produced by NewWave Co., USA. The laser is from ATL Co., Germany. The type of ICP-MS is Agilent 7500a. During the experiment, He was used as the carrier gas of the ablation material. The laser wavelength was 193 nm and the pulse width was less than 4 ns. According to the size of the zircon, the laser beam spot diameter was 35 µm. In the calculation of the Hf mantle model age, the present value of ¹⁷⁶Hf/¹⁷⁷Hf in the depleted mantle is 0.28325 and ¹⁷⁶Lu/¹⁷⁷Hf is 0.0384 [40]. The ¹⁷⁶Lu/¹⁷⁷Hf of average crustal is 0.015 [41].

4. Results

4.1. Major, Rare Earth, and Trace Elements

The ablation of gabbro is slightly higher, ranging from 2.44 to 3.75%. With the lesser influence of later fluid and alteration, the geochemical characteristics can effectively reflect the rock characteristics (Table S1). The SiO₂ content of the sample is 49.72–54.33%, which means intermediate–basic rock. The samples in the TAS diagram (Figure 4a) were placed in the sub-alkaline gabbro and gabbro diorite area, which was the sub-alkaline series of rocks. The rock differentiation index (DI) was 19.47–38.02, and the degree of differentiation was low. The σ_{43} was 0.66–2.03, which was calcic to calc-alkaline rock.

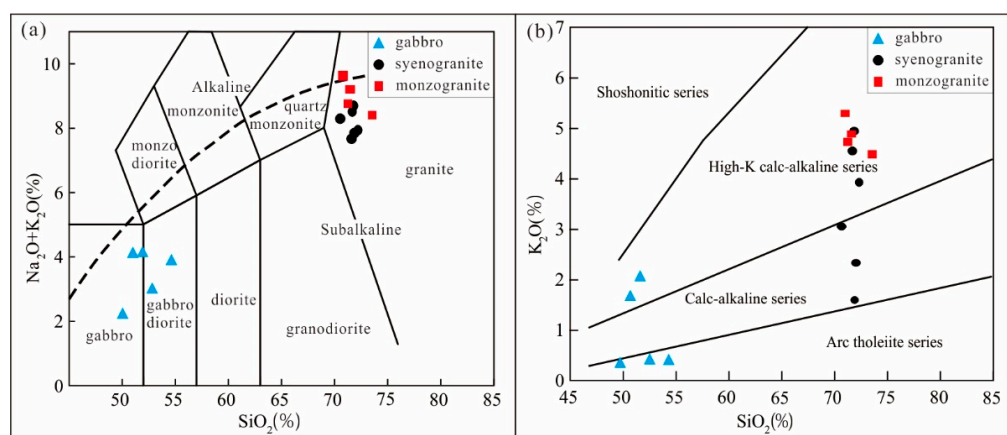


Figure 4. Classification and discriminant diagrams of magmatic rocks. (a)—SiO₂ vs. K₂O+Na₂O plot of intrusive rocks [42]; (b)—K₂O vs. SiO₂ plot [42].

The SiO₂ content of syenogranite samples is 70.63–72.19%, which means acidic rock. In the TAS diagram, the sample was located in the granite area and belonged to the sub-alkaline series (Figure 4a). In the K₂O–SiO₂ diagram (Figure 4b), the sample points were dispersed in the high-K calc-alkaline and calc-alkaline series regions. The DI was 87.02–90.39, and the degree of differentiation was high. The aluminum saturation index

A/CNK was 0.99–1.26, which was a weak–strong peraluminous rock. The SiO₂ content of monzogranite samples is 70.95–73.53%, which indicates acidic rock. In the TAS diagram, the sample was located in the granite area and belonged to the sub-alkaline series (Figure 4a). In the K₂O–SiO₂ diagram (Figure 4b), the sample points were dispersed in the shoshonite and high-K calc-alkaline series. The DI was 89.21–92.55, and the degree of differentiation was high. The A/CNK was 1.05–1.24, which was a strong peraluminous rock.

The rare earth content of gabbro was low. The LREE/HREE ratio was 4.10–5.64, with (La/Yb)_N of 4.27–6.60, and the differentiation degree was slightly small. δ Eu was 1.42–1.72 and positive anomalies were obvious; δ Ce was 0.91–0.94, with a weak negative anomaly. The rare earth distribution curve was slightly rightward. The light rare earth is relatively enriched, and the heavy rare earth is relatively depleted (Figure 5). The trace element content of gabbro rock was slightly lower (Table S1). The trace element spider diagram (Figure 6) showed that the rocks were characterized by relative enrichment of large ion lithophile elements such as Rb, Ba, and K, and loss of high field strength elements, with negative anomalies of Nb and P.

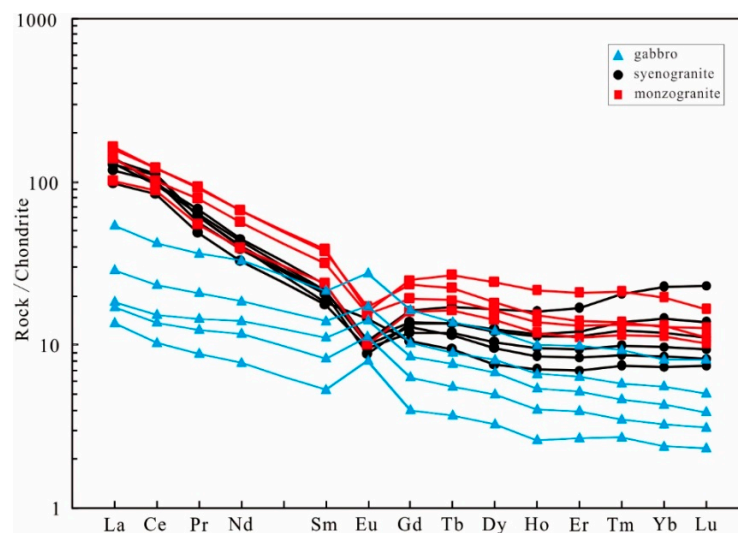


Figure 5. Chondrite-normalized REE patterns of intrusive rocks (normalizing factors are from [43]); Chondrite compositions are from [44].

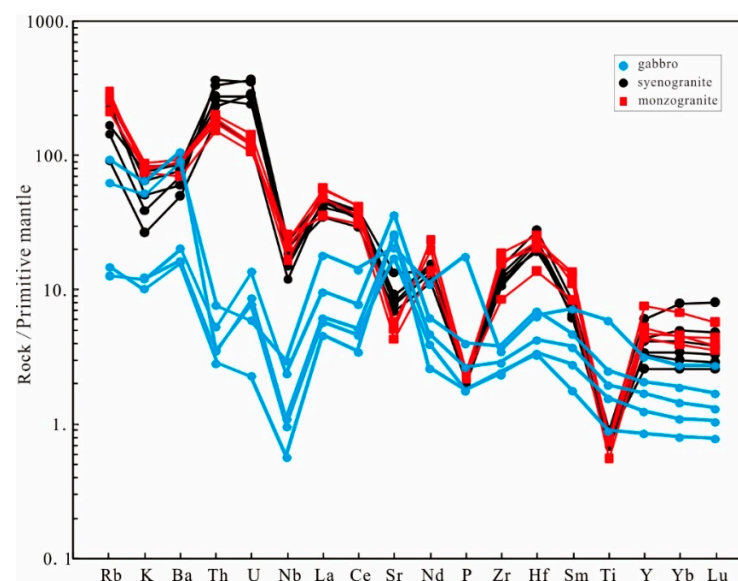


Figure 6. Primitive mantle normalized trace element spider patterns of intrusive rocks (normalizing factors are from [43]); Primitive mantle compositions are from [44].

The ratio of light/heavy rare earth of syenogranite was 7.46–16.84, and $(La/Yb)_N$ was 6.26–18.66. The differentiation degree of light and heavy rare earth was higher; δEu was 0.53–1.04, with a medium–weak negative anomaly; δCe was 1.00–1.24, with a weak positive anomaly. The light/heavy rare earth ratio of monzogranite was 7.48–9.75, and $(La/Yb)_N$ was 8.18–12.66. The differentiation degree of light and heavy rare earth was high. δEu was 0.51–0.62, with a moderate negative anomaly; δCe was 0.97–1.20, with a weak anomaly. The rare earth distribution curve had right-inclined characteristics. The trace element spider diagram (Figure 6) showed that the syenogranite and monzogranite had the characteristics of enrichment in Rb, Ba, Th, and K, and depletion in high field strength elements, with Nb, P, and Ti negative anomalies.

4.2. LA-ICP-MS Zircon U-Pb Ages

The tested zircons had a good degree of idiomorphism, most of which are idiomorphic crystals. The crystal ridges and cone tops of most zircons were corroded and showed to be sub-rounded, with a particle size of 60–120 μm . They had emery lustre, developed oscillatory zoning, and had magmatic genetic characteristics [45]. Zircons without cracks and inclusions were selected for age testing, and points were made at the position of developing oscillatory zones (Figure 7a). The zircon Th/U ratio of DP-141 gabbro was 0.16–0.89 (Table S2), which indicated magmatic zircon (>0.1 ; [46]). The zircon $^{206}Pb/^{238}U$ analysis points of the sample were distributed in a group, and the distribution was relatively concentrated. We removed captured zircons and measuring points with large deviation due to lead loss, the age was concentrated at 809–822 Ma (Figure 7b), and the weighted average was 816.1 ± 4.1 Ma, MSWD = 0.1, N = 20, which was the crystallization age of the pluton, indicating that the gabbro rock mass was formed in the Neoproterozoic era.

The zircon ages of DP-205 syenogranite samples were 620–793 Ma (Figure 7c). The upper intersection point age was 770 ± 13 Ma (MSWD = 1.2), and the weighted average age of zircons of seven measuring points was 783.7 ± 8.1 Ma (MSWD = 1.4) (Figure 7d), indicating that syenogranite pluton was formed in Neoproterozoic. The zircon ages of DP-212 monzogranite samples were 725–776 Ma (Figure 7e). Captured zircons and measuring points with large deviations due to the lead loss were removed, and the weighted average age of zircon was 754.8 ± 6.1 Ma (MSWD = 3.0, N = 23) (Figure 7f), indicating that the monzogranite pluton was also formed in the Neoproterozoic era.

4.3. Zircon Lu-Hf Isotopic Compositions

The $^{176}Lu/^{177}Hf$ ratio of zircons was small, indicating that zircons had only a small amount of radioactive Hf accumulation after formation, so the initial $^{176}Hf/^{177}Hf$ ratio could be used to represent the Hf isotopic composition at the time of formation [47]. The initial $^{176}Lu/^{177}Hf$ ratio and $\epsilon_{Hf}(t)$ value were calculated based on the same zircon U-Pb dating data. The two-stage model age (T_{DM}^C) was calculated based on the depleted mantle source [40]. The results showed that the zircon Hf isotope $^{176}Lu/^{177}Hf$ ratio of the gabbro obtained from 15 test points was relatively stable, from 0.282078 to 0.282440. The $^{176}Yb/^{177}Hf$ ratio was 0.015181–0.04223, with a $f_{Lu/Hf}$ of -0.98 to -0.95 , and the zircon $\epsilon_{Hf}(t)$ was -7.48 – 5.49 , which varied greatly, indicating that the rock might have heterogeneous zircon Hf isotope composition (Figure 8). The zircon Hf single-stage model ages (T_{DM}^C) were 1163.47–1681.76 Ma and the two-stage model ages (T_{DM}^C) were 1590.21–2743.23 Ma.

The zircon Hf isotope $^{176}Lu/^{177}Hf$ of the syenogranite DP-205 was relatively stable, with a ratio of 0.282204–0.282321 (Table S3). The $^{176}Yb/^{177}Hf$ ratio was 0.021570–0.062737; the $f_{Lu/Hf}$ was -0.97 to -0.92 , and the zircon $\epsilon_{Hf}(t)$ was -4.3 to 0.4 (Figure 8). The zircon Hf single-stage model ages (T_{DM}^C) were 1342–1491 Ma, and the two-stage model ages (T_{DM}^C) were 2033–2413 Ma. The zircon Hf isotope $^{176}Lu/^{177}Hf$ ratio of monzogranite DP-212 was 0.28237–0.282608 (Table S3). The $^{176}Yb/^{177}Hf$ ratio was 0.025349–0.078668; the $f_{Lu/Hf}$ was -0.97 to -0.91 , and zircon $\epsilon_{Hf}(t)$ was 1.65–10.36. Zircon Hf single-stage model age (T_{DM}^C) was 926.37–1264.35 Ma and the two-stage model age (T_{DM}^C) was 1120.59–1891.67 Ma.

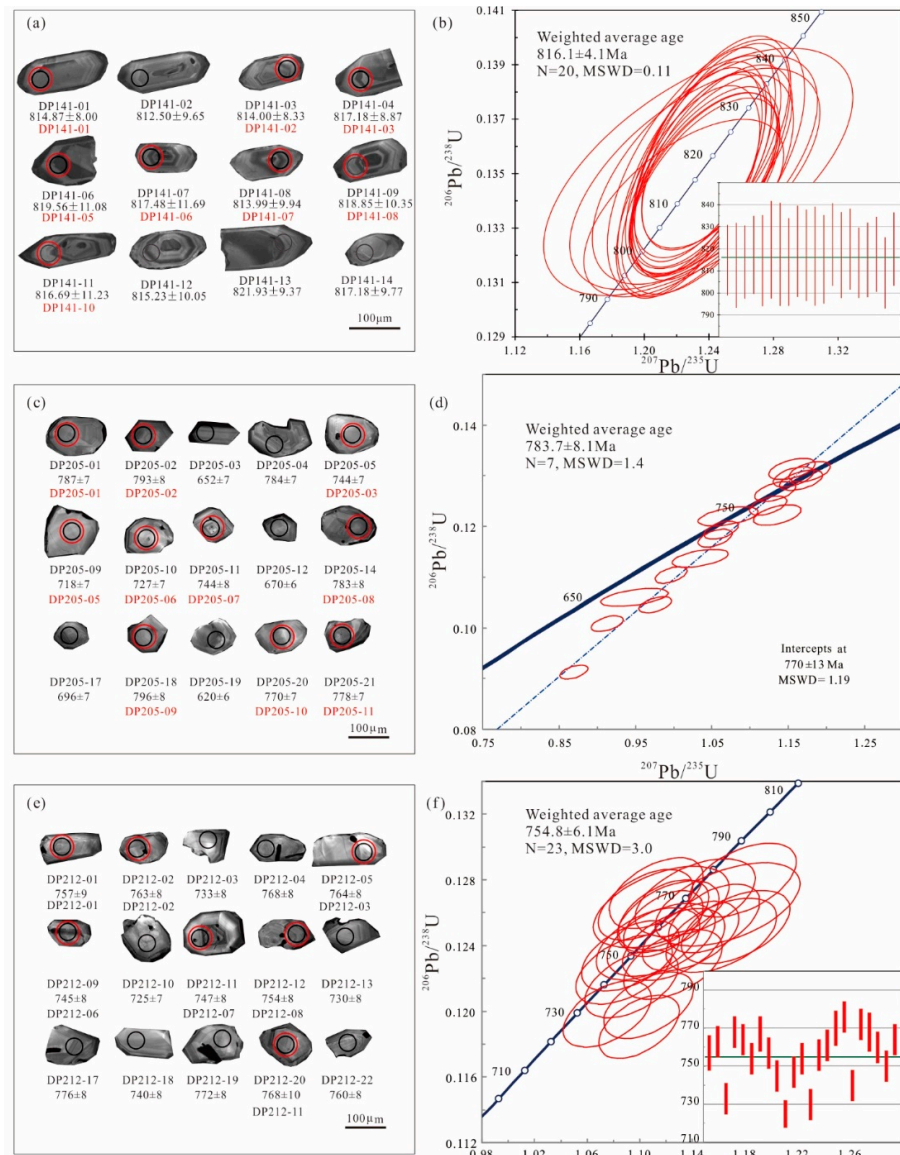


Figure 7. (a)—Cathodoluminescence (CL) images of zircons of the gabbro (DP-141); (b)—LA-ICP-MS zircon U-Pb concordia diagram of the gabbro (DP-141); (c)—Cathodoluminescence (CL) images of zircons of the syenogranite (DP-205); (d)—LA-ICP-MS zircon U-Pb concordia diagram of the syenogranite (DP-205); (e)—Cathodoluminescence (CL) images of zircons of the monzogranite (DP-212); (f)—LA-ICP-MS zircon U-Pb concordia diagram of the monzogranite (DP-212).

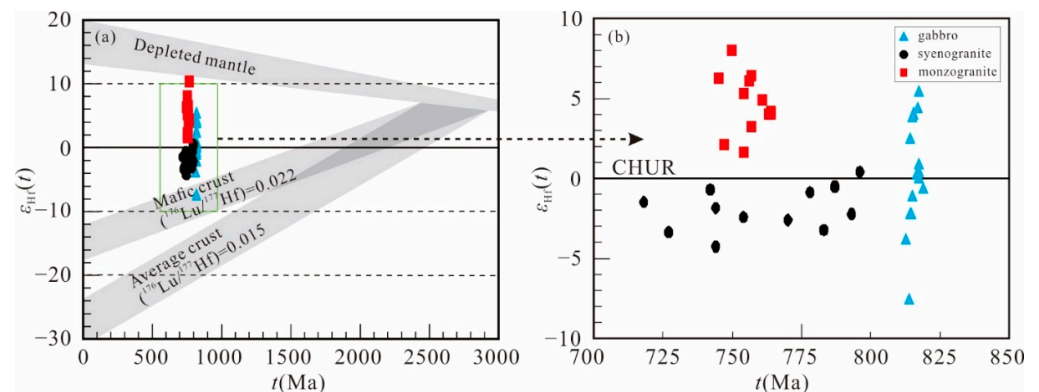


Figure 8. $\epsilon_{Hf}(t)$ versus age diagram ((a), and (b)) (Base image according to [47]).

5. Discussion

5.1. Time Limit of Multi-Period Magmatic Activity

Predecessors obtained multiple sets of different ages of Taohuazhai gabbros by the Rb-Sr isochron method, K-Ar method, and zircon U-Pb method. Using the Rb-Sr isochron method, Han and Jin [23] obtained the gabbro age of 481 Ma. Since the Rb-Sr isotope system has a low closure temperature and is susceptible to later thermal disturbances, the measured age (481 Ma) is more representative of the later thermal event age. Han et al. [25] used K-Ar dating for gabbro and amphibole in it. The whole rock age was 844.63 ± 33.66 Ma, and the amphibole age was 845.25 ± 12.74 to 926.15 ± 94.51 Ma. K-Ar dating also faces defects such as low closure temperature of the isotope system and susceptibility to later thermal disturbance. The age measured is more of a regional tectonic thermal event, which confirms the multi-phase activity characteristics of magmatic activity. Based on a detailed field geological survey, this work selected three representative samples for the isotope age test, to distinguish and classify activity periods of intrusive rocks. Zircon U-Pb dating technology is one of the most mature isotope dating methods. Zircon has the characteristics of easy selection, strong stability, and high closure temperature of isotope systems [48,49].

The weighted average age of gabbro zircon was 816.1 ± 4.1 Ma, MSWD = 0.114; the upper intersection age of syenogranite was 770 ± 13 Ma, with a weighted average age of 783.7 ± 8.1 Ma; The weighted average age of monzogranite was 754.8 ± 6.1 Ma, indicating that the Daping pluton was the product of Neoproterozoic magmatic activity. These zircon U-Pb ages were different from the previously measured zircon U-Pb ages (773 ± 12 Ma, [26]; 761.6 ± 7.4 Ma, [27]). The K-Ar ages measured by Han et al. [25] were older than the measured zircon ages, indicating that the Taohuazhai gabbro was the product of multiple stages of magmatic activity. The discrete ages of 1034 ± 10 Ma, 1063 ± 10 Ma, and 925 ± 11 Ma obtained from this dating were larger than the crystallization age of magma, which might be the early captured zircons. The Neoproterozoic magmatic activity in the Daping area was mainly divided into two stages. The first stage was mainly the intrusion of gabbro (~810 Ma), and the second stage was the joint intrusion of gabbro, syenogranite, and monzogranite (780–750 Ma).

5.2. Rodinia Breakup and Magmatic Response

The syenogranites and monzogranites were highly fractionated granites, and the P_2O_5 was lower, which was different from the highly differentiated S-type granites [50]. The syenogranite and monzogranite had high FeO^T (1.69–2.37% and 1.19–1.51%) and A-type granite characteristics (higher than 1%) [51]. They were characterized by low Rb and high Ba, which was inconsistent with the characteristics of highly differentiated I-type granite [51]. Comprehensive analysis showed that syenogranite and monzogranite were A-type granite. A-type granites were produced in rift zones and stable continental plates. These rocks were usually weakly alkaline granites, mainly formed in an extensional tectonic setting, and were important indicators of tectonic environment identification. In the Nb-Y-Ce diagram of A-type granites (Figure 9), the samples dropped in the post-orogenic (post-collisional) region of A_2 , close to the intraplate region of A_1 , with transitional properties.

The Ba/Th ratios of syenogranite and monzogranite were 13.58–27.33 and 37.30–41.69, respectively, which were far less than 300, indicating that the magma sources were not affected by subduction zone fluids [52,53]. The formation environment was not related to the arc tectonic environment under the subduction background. The Rb-Yb-Ta diagram (Figure 10a) showed that the samples were placed in the post-collision tectonic environment. The Ta-Yb diagram (Figure 10b) showed that the samples were placed near the post-collision tectonic environment and its boundary. There were no or very few residual garnets in the magma source of syenogranite and monzogranite in this area. The Y/Yb ratios were 7.10–10.29 and 9.62–10.72, respectively, close to 10 [54], and the HREE distribution curve was flat [55], indicating that the magma source area was dominated by hornblende. The syenogranite and monzogranite have negative δEu anomalies, indicating that the magma source area had stable plagioclase residues. The δCe values were 1.00–1.24 and 0.97–1.20,

indicating that the magma source area was oxidized. Through the above analysis, it was considered that the mineral assemblage of syenogranite and monzogranite magma source area was hornblende+plagioclase, which was shallow in formation depth, low in pressure, and developed in an intracontinental rift environment.

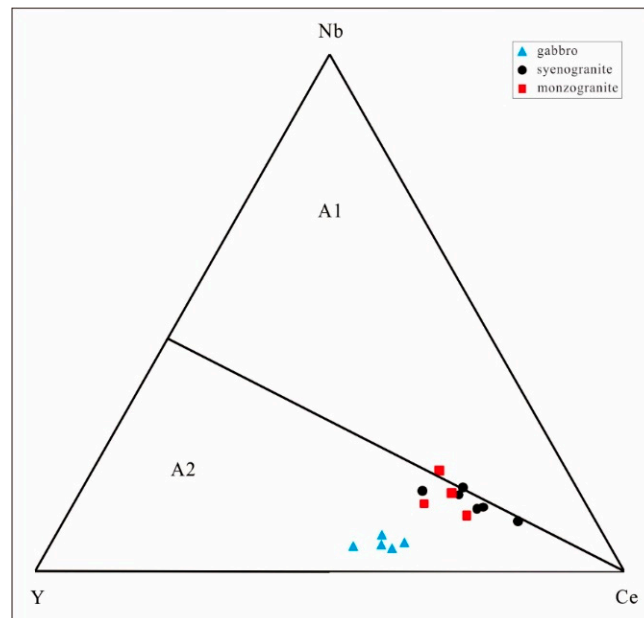


Figure 9. RB versus YB + Ta diagram of intrusive rocks (Base image according to [56]).

The zircon $\varepsilon_{\text{Hf}}(t)$ of the gabbro was -7.48 – 5.49 and the range of variation was large, mainly negative. The Hf two-stage model age (T_{DM}^{C}) is 1590.21 – 2743.23 Ma, indicating that the magma source area was the mainly ancient crust source material, and a small amount of positive $\varepsilon_{\text{Hf}}(t)$ indicated that there was new mantle source material in that period, which reflected that it had the characteristics of rift magmatic rock. The rock had a positive δEu anomaly (1.42 – 1.72), indicating that the rock was formed in a low-pressure extensional environment. The $\varepsilon_{\text{Hf}}(t)$ of syenogranite was mainly negative and the $\varepsilon_{\text{Hf}}(t)$ of monzogranite was positive. The zircon Hf isotope characteristics of syenogranite showed that the magma source area was mainly composed of ancient continental crust (Ailaoshan Group), with a small number of mantle-derived components. The zircon $\varepsilon_{\text{Hf}}(t)$ of monzogranite was 1.65 – 10.36 , indicating that the magma source area contains a large number of mantle-derived components. The two-stage model age (T_{DM}^{C}) was 1120.59 – 1891.67 Ma, and the variation range was large, indicating that the magma source area had contributed to ancient crustal material (Ailaoshan Group). The Nb/Ta ratios of syenogranite and monzogranite were 6.65 – 12.00 and 6.72 – 10.50 , respectively, and the variation range was large, indicating that the magma source area was a mixed source [57–59]. Previous Sr and Nd isotope studies have shown that the magma source of monzogranite was crust–mantle mixing [60].

The breakup time of the Rodinia varied at different locations. Paleomagnetic data showed that the Laurasia Plate, the South China ancient land, and the Australia–Antarctic ancient land began to disintegrate at 830 Ma, and the Rodinia remained for at least 725 Ma when separated [5]. Torsvik et al. [61] believed that the disintegration time of Rodinia was 725 – 750 Ma. Intraplate non-orogenic magmatic rocks in Neoproterozoic (830 – 800 Ma and 780 – 750 Ma) may be related to the mantle plume/super mantle plume activity that led to the breakup of Rodinia [62–67]. The Suxiong Formation was formed in a rift environment [3,62]. The rifting between the western margin of the Yangtze Plate and the Cathaysian Plate began from 830 – 820 Ma and the peak period of rifting was about 810 Ma [9,16,51,68]. The above data showed that in the age range of 830 – 750 Ma, the rocks formed around the Yangtze block were under the continental margin rift tectonic background, and there were mainly two stages (830 – 800 Ma and 780 – 750 Ma) of magmatic response to the Rodinia breakup.

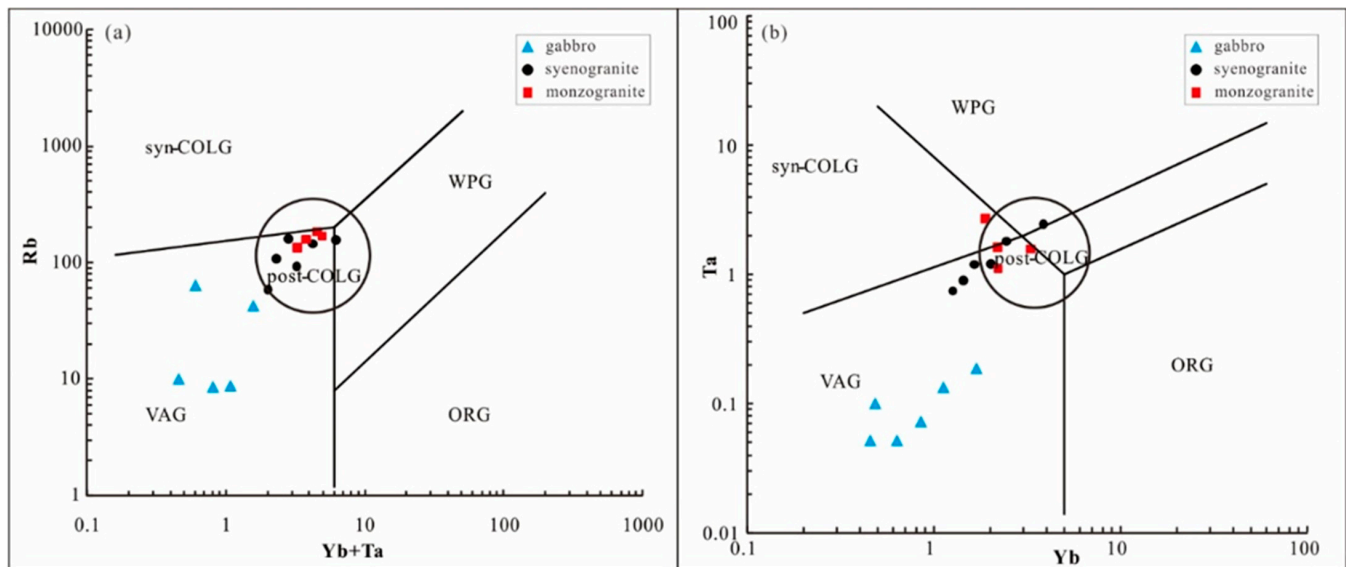


Figure 10. Tectonic discrimination diagrams for magmatic rocks (Base image according to [69]). (a)—Rb vs.(Yb + Ta) diagram; (b)—Ta vs. Yb diagram. Syn-COLG, syn-collision granite; VAG, volcanic arc granite; WPG, within plate granite; ORG, ocean ridge granite; Post-COLG, post-collision granite.

In conclusion, the regional research results, combined with the zircon U-Pb geochronology and Lu-Hf isotopic characteristics of the two types of intrusive rocks, suggested that the granites and gabbros were formed in a continental rift environment, corresponding to the two-stage magmatic response of the Rodinia breakup, respectively. At the same time, it indicated that the Ailaoshan area on the southwestern margin of the South China Plate in the early Neoproterozoic era was in a rift tensile environment, where the Rodinia breakup began at 816 Ma and lasted at least until 755 Ma. The close relationship between the Neoproterozoic intrusive rocks and the Rodinia breakup event provides an important guide for further research and exploration work in the region.

6. Conclusions

Based on the regional geology, geochemistry, and isotopic studies of zircons associated with gabbros and granites in the Daping area, the following conclusions have been made:

(1) The gabbro, syenogranite, and monzogranite of the Daping pluton are sub-alkaline series rocks, which were formed in a transitional tectonic environment of post-collision to intraplate continental margin rift.

(2) The weighted average age of the gabbro was 816.1 ± 4.1 Ma; the weighted average age of syenogranite was 783.7 ± 8.1 Ma, and that of the monzogranite was 754.8 ± 6.1 Ma, all of which were formed in the Neoproterozoic era.

(3) The gabbro magma source was mainly derived from ancient crust source materials and new mantle source materials; the magma source area of syenogranite was ancient continental crust (Ailaoshan Group) and a few depleted mantle materials, and a large number of mantle-derived components composed the monzogranite magma source area.

(4) The ages of the Daping pluton indicated that the Rodinia breakup began at 816 Ma and lasted at least until 755 Ma in the Ailaoshan orogenic belt.

Supplementary Materials: The following supporting information can be downloaded at: <https://www.mdpi.com/article/10.3390/min13030349/s1>, Table S1: Major element (wt%), REE element (ppm), and trace element (ppm) compositions of magmatic rocks; Table S2: LA-ICP-MS zircon U-Pb data of magmatic rocks; Table S3: LA-ICP-MS Lu-Hf analysis results of the magmatic rock zircons [70,71].

Author Contributions: Conceptualization, Y.Z. and D.Z.; methodology, X.M. and K.L.; software, S.W.; validation, Z.Z. and X.H.; formal analysis, T.Y.; investigation, Y.Z., S.W. and D.Z.; resources, D.Z. and S.W.; data curation, S.W.; writing—original draft preparation, Y.Z. and S.W.; writing—review and editing, D.Z. and X.M.; visualization, K.L.; supervision, X.M. and D.Z.; project administration, K.L. and X.H.; funding acquisition, D.Z. and K.L. All authors have read and agreed to the published version of the manuscript.

Funding: This study was supported by the fundamental research funds of China Geological Survey Research (JKY202004) and the project of China Geological Survey (DD20221677-2).

Data Availability Statement: Not applicable.

Acknowledgments: We are grateful for the assistance during fieldwork provided by Jun Liu from Huaxi Gold Co., Ltd., Yuanyang, Yunnan, China. The authors also thank Lele Han of China University of Geosciences (Beijing) for the computer mapping work.

Conflicts of Interest: The authors declare no conflict of interest.

References

1. McMenamin, M.A.S.; McMenamin, D.L.S. *The Emergence of Animals: The Cambrian Breakthrough*; Columbia University Press: New York, NY, USA, 1990; pp. 1–12.
2. Hoffman, P.F. Did the breakup of Laurentia turn Gondwana inside out? *Science* **1991**, *252*, 1409–1412. [[CrossRef](#)] [[PubMed](#)]
3. Li, Z.X.; Zhang, L.H.; Powell, C.M. South China in Rodinia: Part of the missing link between Australia-East Antarctic and Laurentia. *Geology* **1995**, *23*, 407–410. [[CrossRef](#)]
4. Li, Z.X.; Zhang, L.H.; Powell, C.M. Positions of the East Asian cratons in the Neoproterozoic super-continent Rodinia. *Aust. Earth Sci.* **1996**, *43*, 593–604. [[CrossRef](#)]
5. Powell, C.M.; Li, Z.X.; Mc Elhinny, M.W. Paleomagnetic constrains on timing of the Neoproterozoic breakup of Rodinia and the Cambrian formation of Gondwana. *Geology* **1993**, *21*, 889–892. [[CrossRef](#)]
6. Fanning, C.M.; Daly, S.J.; Bennett, V.B.; Menot, R.P.; Monnier, O. The Mawson Continent: Archean to Proterozoic Crust in the East Antarctic Shield and Gawler Craton, Australia. A Cornerstone in Rodinia and Gondwanaland. In *Abstracts-Geological Society of Australia*; Geological Society of Australia: Sydney, NSW, Australia, 1996; Volume 41, p. 135.
7. Fanning, C.M.; Rankin, L.R. Magmatic and tectonic evolution of the southern Gawler Craton; new data on timing from U-Pb isotopic. *Abstr. Geol. Soc. Aust.* **1994**, *36*, 40–41.
8. Li, X.H.; Li, W.X.; Li, Z.X.; Ying, L. 850–790Ma bimodal volcanic and intrusive rocks in northern Zhejiang, South China: A major episode of continental rift magmatism during the breakup of Rodinia. *Lithos* **2008**, *102*, 341–357. [[CrossRef](#)]
9. Wang, J.; Liu, B.J.; Pan, G.T. Neoproterozoic rifting history of South China significance to Rodinia break up. *J. Pet.* **2001**, *21*, 135–145. (In Chinese with English Abstract)
10. Wang, J. *Neoproterozoic Rifting History of South China: Significance to Rodinia Breakup*; Geological Publication House: Beijing, China, 2000; pp. 1–146. (In Chinese)
11. Wang, X.C.; Li, X.H.; Li, W.X.; Li, Z.X. 825Ma komatiitic basalts in South China: First evidence for >1500°C mantle melts by a Rodinian mantle plume. *Geology* **2007**, *35*, 1103–1106. [[CrossRef](#)]
12. Li, Z.X.; Li, X.H.; Zhou, H.W.; Peter, D.K. Grenvillian continental collision in south China: New SHRIMP U-Pb zircon results and implications for the configuration of Rodinia. *Geology* **2002**, *30*, 163–166. [[CrossRef](#)]
13. Wang, X.C.; Li, X.H.; Li, W.X.; Li, Z.X.; Liu, Y.; Yang, Y.H.; Liang, X.R.; Tu, X.L. The Bikou basalts in the northwestern Yangtze block, South China: Remnants of 820–810Ma continental flood basalts? *GSA Bull.* **2008**, *120*, 1478–1492. [[CrossRef](#)]
14. Ling, W.L.; Gao, S.; Zhang, B.R.; Li, H.M.; Liu, Y.; Cheng, J.P. Neoproterozoic tectonic evolution of the northwestern Yangtze craton, South China: Implications for amalgamation and break-up of the Rodinia Supercontinent. *Precambrian Res.* **2003**, *122*, 111–140. [[CrossRef](#)]
15. Li, H.K.; Lu, S.N.; Chen, Z.H.; Xiang, Z.Q.; Hao, G.J. Zircon U-Pb geochronology of rift-type volcanic rocks of the Yaolinghe Group in the South Qinling orogen. *Geol. Bull. China* **2003**, *22*, 775–781. (In Chinese with English Abstract)
16. Li, X.H.; Wang, X.C. Petrogenesis and tectonic significance of Neoproterozoic basaltic rocks in South China: From orogenesis to intracontinental rifting. *Geochimica* **2008**, *37*, 382–398.
17. Yang, J.S.; Shi, R.D.; Wu, C.L.; Chen, S.Y. Recognition of Neoproterozoic ophiolite on the northern margin of the Qaidam basin: Evidence of the breakup of Rodinia. *Geol. Bull. China* **2004**, *23*, 892–898. (In Chinese with English Abstract)
18. Zhou, J.B.; Li, X.H.; Ge, W.C.; Li, Z.X. Age and origin of middle Neoproterozoic mafic magmatism in southern Yangtze Block and relevance to the break-up of Rodinia. *Gondwana Res.* **2007**, *12*, 184–197. [[CrossRef](#)]
19. Zhu, W.G.; Zhong, H.; Li, X.H.; Deng, H.L.; He, D.F.; Wu, K.W.; Bai, Z.J. SHRIMP zircon U-Pb geochronology, elemental, and Nd isotopic geochemistry of the Neoproterozoic mafic dykes in the Yanbian area, SW China. *Precamb Res.* **2008**, *164*, 66–85. [[CrossRef](#)]
20. Du, Q.D.; Wang, J.; Wang, Z.J.; Deng, Q.; Yang, F. Depositional Differentiation and Provenance Analysis of Liantuo Formation in Neoproterozoic Rift Basin, Yangtze Block. *Earth Sci.* **2021**, *46*, 2530–2541. (In Chinese with English Abstract)

21. Xu, Y.W.; Li, C.D.; Zhao, L.G.; Sun, H.Y.; Xu, T.; Teng, X.M. Bimodal Volcanic Rocks of Dingyuan Formation on the Northern Margin of Dabie Belt: A Witness of Late Neoproterozoic Rifting Event. *Earth Sci.* **2020**, *46*, 2732–2750. (In Chinese with English Abstract)
22. Cai, Y.; Wang, Y.; Cawood, P.A.; Fan, W.; Liu, H.; Xing, X.; Zhang, Y. Neoproterozoic subduction along the Ailaoshan zone, South China: Geochronological and geochemical evidence from amphibolite. *Precambrian Res.* **2014**, *245*, 13–28. [[CrossRef](#)]
23. Han, R.S.; Jin, S.C. Genesis and Criteria for Ore prospecting in the Yuanyang gold deposit, Yunan province. *Geol. Explor. Nonferrous Met.* **1994**, *3*, 218–222. (In Chinese with English Abstract)
24. Ying, H.L. The Geochemistry characteristics of wallrock alteration and Isotopes of the Dahe Geochemistry. *Gold Sci. Technol.* **1998**, *6*, 14–23. (In Chinese)
25. Han, R.S.; Jin, S.C.; Lei, L. Geochemistry of Ore-forming hydrothermal system of Daping reworked gold deposit, Yuanyang, Yunan. *Acta Mineral. Acta Mineral. Sin.* **1997**, *03*, 337–344. (In Chinese with English Abstract)
26. Zhang, Y.; Sun, X.M.; Shi, G.Y.; Xiong, D.X.; Zhai, W.; Pan, W.J.; Hu, B.M. SHRIMP U-Pb dating of zircons from diorite batholith hosting Daping gold deposit in Ailaoshan gold belt, Yunan Province, China. *Acta Petrol. Sin.* **2011**, *27*, 2600–2608. (In Chinese with English Abstract)
27. Chen, Y.H. Metallogenic Conditions and Gold Enrichment Regularity in the Daping Gold Deposit, Yunnan Province, P.R. China. Ph.D. Thesis, China University of Geosciences, Wuhan, China, 2015. (In Chinese).
28. Deng, J.; Hou, Z.Q.; Mo, X.X.; Yang, L.Q.; Wang, C.M. Superimposed orogenesis and metallogenesis in Sanjiang Tethys. *Miner. Deposits.* **2010**, *29*, 37–42.
29. Deng, J.; Wang, C.M.; Bagas, L.; Selvaraja, V.; Yang, L. Insights into ore genesis of the Jinding Zn-Pb deposit, Yunnan Province, China: Evidence from Zn and in-situ S isotopes. *Ore Geol. Rev.* **2017**, *90*, 943–957. [[CrossRef](#)]
30. Deng, J.; Wang, Q.F.; Li, G.J.; Li, C.S.; Wang, C.M. Tethys tectonic evolution and its bearing on the distribution of important mineral deposits in the Sanjiang region, SW China. *Gondwana Res.* **2014**, *26*, 419–437. [[CrossRef](#)]
31. Wang, C.M.; Zhang, D.; Wu, G.G.; Santosh, M.; Zhang, J.; Xu, Y.G.; Zhang, Y.Y. Geological and isotopic evidence for a magmatic-hydrothermal origin of the Ag-Pb-Zn deposits in the Lengshuikeng district, east-central China. *Miner. Deposita.* **2014**, *49*, 733–749. [[CrossRef](#)]
32. Yang, L.F.; Shi, K.X.; Wang, C.M. Ore genesis of the Jinman Copper deposit in the Lanping Basin, Sanjiang Orogen: Constraints by copper and sulfur isotopes. *Acta Petrol. Sin.* **2016**, *32*, 2392–2406. (In Chinese with English Abstract)
33. Zhang, Y.Y.; Liu, K.; Wang, Y.; Zhang, D.; Mo, X.X.; Deng, Y.F.; Yu, T.X.; Zhao, Z.N. Geological significance of Late Permian magmatic rocks in the middle section of the Ailaoshan orogenic belt, SW China: Constraints from petrology, geochemistry and geochronology. *Minerals.* **2022**, *12*, 652. [[CrossRef](#)]
34. Wang, C.M.; Deng, J.; Santosh, M.; Carranza, E.J.M.; Gong, Q.J.; Guo, C.Y.; Xia, R.; Lai, X.R. Timing, tectonic implications and genesis of gold mineralization in the Xincheng gold deposit, China: C-H-O isotopes, pyrite Rb-Sr and zircon fission track thermochronometry. *Ore Geol. Rev.* **2015**, *65*, 659–673. [[CrossRef](#)]
35. Du, B.; Wang, C.M.; He, X.Y.; Yang, L.F.; Chen, J.Y.; Shi, K.X.; Luo, Z.; Xia, J.S. Advances in research of bulk-rock Nd and zircon Hf isotopic mappings: Case study of the Sanjiang Tethyan Orogen. *Acta Petrol. Sin.* **2016**, *32*, 2555–2570. (In Chinese with English abstract).
36. Wang, M.L.; Zhnag, J.G.; Wang, X.W.; Luan, Q.L. Characteristics of paleotectonic stress filed on the ailaoshan structural belt. *J. Geomech.* **2014**, *20*, 82–91. (In Chinese with English Abstract)
37. Sláma, J.; Košler, J.; Condon, D.J.; Crowley, J.L.; Gerdes, A.; Hanchar, J.M.; Horstwood, M.S.; Morris, G.A.; Nasdala, L.; Norberg, N. Plešovice zircon-A new natural reference material for U-Pb and Hf isotopic microanalysis. *Chem. Geol.* **2008**, *249*, 1–35. [[CrossRef](#)]
38. Andersen, T. Correction of common lead in U-Pb analyses that do not report ²⁰⁴Pb. *Chem. Geol.* **2002**, *192*, 59–79. [[CrossRef](#)]
39. Liu, Y.S.; Hu, Z.C.; Zong, K.Q.; Gao, C.G.; Gao, S.; Juan, X.U.; Chen, H.H. Reappraisal and refinement of zircon U-Pb isotope and trace Geotectonica element analyses by LA-ICP-MS. *Chin. Sci. Bull.* **2010**, *55*, 1535–1546. (In Chinese with English Abstract) [[CrossRef](#)]
40. Griffin, W.L.; Pearson, N.J.; Belousova, E.; Jackson, S.E.; Achterbergh, E.; O'Reilly, S.Y.; Shee, S.R. The Hf isotope composition of cratonic mantle: LAM-MC-ICPMS analysis of zircon megacrysts in kimberlites. *Geochim. Cosmochim. Acta* **2000**, *64*, 133–147. [[CrossRef](#)]
41. Griffin, W.L.; Wang, X.; Jackson, S.E.; Pearson, N.J.; O'Reilly, S.Y.; Xu, X.S.; Zhou, X.M. Zircon chemistry and magma mixing, SE China: In-situ analysis of Hf isotopes, Tonglu and Pingtan igneous complexes. *Lithos* **2002**, *61*, 237–269. [[CrossRef](#)]
42. Middlemost, E.A.K. Naming materials in the magma/igneous rock system. *Earth Sci. Rev.* **1994**, *37*, 215–224. [[CrossRef](#)]
43. Boynton, W.V. Cosmochemistry of the Rare Earth Elements: Meteorite Studies. In *Rare Earth Element Geochemistry*; Henderson, P., Ed.; Elsevier: Amsterdam, The Netherlands, 1984; pp. 63–114.
44. Sun, S.S.; McDonough, W.F. Chemical and isotopic systematics of oceanic Basalts: Implications for mantle composition and processes. In *Magmatism in the Ocean Basins*; Saunders, A.D., Norry, M.J., Eds.; Geological Society, London, Special Publications: Bath, UK, 1989; Volume 42, pp. 313–345.
45. Rubatto, D.; Gebauer, D. Use of cathodoluminescence for U-Pbzircon dating by IOM Microprobe: Some examples form the western Alps. In *Cathodoluminescence in Geosciences*; Springer: Berlin/Heidelberg, Germany, 2000; pp. 373–400.
46. Cleasson, S.; Vetrin, V.; Bayanova, T.; Downes, H. U-Pb zircon ages from a Devonian carbonatite dyke, Kola peninsula, Russia: A record of geological evolution from the Archaean to the Palaeozoic. *Lithos* **2000**, *51*, 95–108. [[CrossRef](#)]

47. Wu, F.Y.; Li, X.H.; Zheng, Y.F.; Gao, S. Lu-Hf isotopic systematics and their application in petrology. *Acta Petrol. Sin.* **2007**, *2*, 185–220. (In Chinese with English Abstract)
48. Lee, J.; Williams, I.; Ellis, D. Pb, U and Th diffusion in nature Zircon. *Nature* **1997**, *390*, 159–162. [[CrossRef](#)]
49. Wu, Y.B.; Zheng, Y.F. Zircon genetic mineralogy and its constraints on U-Pb age interpretation. *Chin. Sci. Bull.* **2004**, *49*, 1589–1604. (In Chinese with English Abstract) [[CrossRef](#)]
50. King, P.L.; White, A.J.R.; Chappell, B.W. Characterization and origin of a luminous A type granites of the Lachlan Fold Belt, southeastern Australia. *J. Petrol.* **1997**, *36*, 371–391. [[CrossRef](#)]
51. Wang, Q.; Zhao, Z.H.; Xiong, X.L. A Method for Estimating the Degree and Mass of Magma Degassing during the Volcanic Eruption and Its Application. *Acta Petrol. et Mineral.* **2000**, *19*, 297–306. (In Chinese with English Abstract)
52. Brenan, J.M.; Shaw, H.F.; Ryerson, F.J.; Phinney, D.L. Mineral aqueous fluid partitioning of trace elements at 900 °C and 2.0GPa: Constraints on the trace element chemistry of mantle and deeper crustal fluids. *Geochim. et Cosmochim. Acta* **1995**, *59*, 3331–3350. [[CrossRef](#)]
53. Devine, J.D. Petrogenesis of the basalt-andesite-dacite association of Grenada, Lesser Antilles Island. *Arc. J. Volcanol. Geotherm. Res.* **1995**, *69*, 1–33. [[CrossRef](#)]
54. Ge, X.Y.; Li, X.H.; Chen, Z.G.; Li, W.P. Geochemical characteristics, and genesis of Yanshanian high Sr low Y medium acid volcanic rocks in eastern China: Constraints on crustal thickness in eastern China. *Chin. Sci. Bull.* **2002**, *47*, 474–480. (In Chinese with English Abstract)
55. Zhang, Q.; Wang, Y.; Li, C.D.; Wang, Y.L.; Jin, W.J.; Jia, X.Q. Granite classification on the basis of Sr and Yb contents and its implications. *Acta Petrol. Sin.* **2006**, *22*, 2249–2269. (In Chinese with English Abstract)
56. Eby, G.N. Chemical subdivision of the A-type granitoids: Petrogenetic and tectonic implications. *Geol.* **1992**, *20*, 641–644. [[CrossRef](#)]
57. Foley, S.F. Liquid immiscibility and melt segregation in alkaline lamprophyres from Labrador. *Lithos.* **1984**, *17*, 127–137. [[CrossRef](#)]
58. Barth, M.G.; McDonough, W.F.; Rudnick, R.L. Tracking the budget of Nb and Ta in the continental crust. *Chem. Geol.* **2000**, *165*, 197–213. [[CrossRef](#)]
59. Wedepohl, K.H. The composition of the continental crust. *Geochim. et Cosmochimica Acta* **1995**, *59*, 1217–1232. [[CrossRef](#)]
60. Wang, Z.H.; Guo, X.D.; Ge, L.S.; Wang, L.; Chang, C.J.; Cong, R.X.; Zhang, H.Y. Geochemical characteristics of monzonite granite from the Daping gold mining area, Yunnan Province and geological significance. *Geol. Exploration.* **2012**, *48*, 618–628. (In Chinese with English Abstract)
61. Torsvik, T.H.; Lohmann, K.C.; Sturt, B.A. Verdian glaciations and their relation to the dispersal of Rodinia: Paleomagnetic: A tale of Baltica and Laurentia. *Earth Sci. Rev.* **1996**, *40*, 229–258. [[CrossRef](#)]
62. Li, X.H.; Zhou, H.W.; Li, Z.X. Zircon U-Pb age and petrochemical characteristics of the neoproterozoic bimodal volcanics from western Yangtze block. *Geochim.* **2001**, *30*, 315–322.
63. Li, X.H.; Li, Z.X.; Ge, W.C.; Zhou, H.W.; Li, W.X.; Liu, Y.; Wingate, M.T.D. Neoproterozoic granitoids in South China: Crustal melting above a mantle plume at ca. 825Ma? *Precambrian Res.* **2003**, *122*, 45–83. [[CrossRef](#)]
64. Li, X.H.; Li, Z.X.; Zhou, H.W.; Liu, Y.; Kinny, P.D. U-Pb zircon geochronology, geochemistry and Nd isotopic study of Neoproterozoic bimodal volcanic rocks in the Kangdian Rift of South China: Implications for the initial rifting of Rodinia. *Precambrian Res.* **2002**, *113*, 135–154. [[CrossRef](#)]
65. Li, Z.X.; Li, X.H.; Kinny, P.D.; Wang, J. The breakup of Rodinia: Did it start with a mantle plume beneath South China? *Earth Planet Sci. Lett.* **1999**, *173*, 171–181. [[CrossRef](#)]
66. Li, Z.X.; Li, X.H.; Kinny, P.D.; Wang, J.; Zhang, S.; Zhou, H. Geochronology of Neoproterozoic syn-rift magmatism in the Yangtze Craton, South China, and correlations with other continents: Evidence for a mantle superplume that broke up Rodinia. *Precambrian Res.* **2003**, *122*, 85–109. [[CrossRef](#)]
67. Xia, L.Q.; Xia, Z.C.; Li, X.M.; Ma, Z.P.; Xu, X.Y. Mid-Neoproterozoic Rift-related Volcanic Rocks in South China: Geological Records of Rifting and Break-up of the Supercontinent Rodinia. *Northwestern. Geol.* **2009**, *42*, 1–33.
68. Wang, X.L.; Zhou, J.C.; Qiu, J.S.; Gao, J.F. Petrogenesis of Neoproterozoic peraluminous granites from northeastern Hunan Province: Chronological and Geochemical Constraints. *Geol. Rev.* **2004**, *50*, 65–76. (In Chinese with English Abstract)
69. Pearce, J.A.; Harris, N.B.W.; Tindle, A.G. Trace element discrimination diagrams for the tectonic interpretation of granitic rocks. *J. Petrol.* **1984**, *25*, 956–983. [[CrossRef](#)]
70. Soderlund, U.; Patchett, P.J.; Vervoort, J.D.; Isachsen, C.E. The ¹⁷⁶Lu decay constant determined by Lu-Hf and U-Pb isotope systematic of Precambrian mafic intrusions. *Earth Planet Sci. Lett.* **2004**, *219*, 311–324. [[CrossRef](#)]
71. Blichert-Toft, J.; Chauvel, C.; Albarède, F. Separation of Hf and Lu for high-precision isotope analysis of rock samples by magnetic sector-multiple collector ICP-MS. *Contrib. Mineral. Petrol.* **1997**, *127*, 248–260. [[CrossRef](#)]

Disclaimer/Publisher’s Note: The statements, opinions and data contained in all publications are solely those of the individual author(s) and contributor(s) and not of MDPI and/or the editor(s). MDPI and/or the editor(s) disclaim responsibility for any injury to people or property resulting from any ideas, methods, instructions or products referred to in the content.